AIP | Physics of Fluids

On the stabilizing effects of neck-in, gravity, and inertia in Newtonian film casting

M. Bechert, D. W. Schubert, and B. Scheid

Citation: Physics of Fluids **28**, 024109 (2016); doi: 10.1063/1.4941762
View online: http://dx.doi.org/10.1063/1.4941762
View Table of Contents: http://scitation.aip.org/content/aip/journal/pof2/28/2?ver=pdfcov
Published by the AIP Publishing

PHYSICS OF FLUIDS **28**, 024109 (2016)

On the stabilizing effects of neck-in, gravity, and inertia in Newtonian film casting

M. Bechert,[1,a)] D. W. Schubert,[1] and B. Scheid[2]
[1]*Institute of Polymer Materials, Friedrich-Alexander-Universität Erlangen-Nürnberg, Martensstr. 7, 91058 Erlangen, Germany*
[2]*TIPs, Université Libre de Bruxelles C.P. 165/67, 1050 Brussels, Belgium*

(Received 12 October 2015; accepted 23 January 2016; published online 17 February 2016)

We investigate the influence of the reduction of width along the stretching direction, the so-called neck-in effect, on the draw resonance instability in Newtonian film casting using a linear stability analysis of a model of reduced dimensionality including gravity and inertia forces. Proper scaling reveals the aspect ratio, i.e., the ratio of the initial film half-width to the film length, together with the fluidity and the inlet velocity as independent, dimensionless control parameters. Moreover, we introduce the local Trouton ratio as a measure for the type of elongational deformation, which can be uniaxial, planar, or a combination of both. In the case of purely uniaxial or planar deformations, a one-dimensional model is sufficient. The influence of the control parameters on the draw resonance instability, including a threshold to unconditional stability, is visualized by several stability maps. Special cases of viscous-gravity and viscous-inertia models are analyzed separately due to their practical importance. Gravity appears to influence the aspect ratio at which the critical draw ratio is maximum and amplifies the stabilizing effect of the neck-in. Inertia increases the stabilization due to neck-in, eventually leading to a window of unconditional stability within the analyzed region of aspect ratios. The mechanism underlying the complete suppression of draw resonance is presented, using exclusively steady state analysis. Additionally, the stabilizing mechanisms of gravity and neck-in are revealed. Known alternative stability criteria are extended to the case of finite width and their validity is tested in the presence of inertia, gravity, and finite aspect ratios. © *2016 AIP Publishing LLC.* [http://dx.doi.org/10.1063/1.4941762]

I. INTRODUCTION

The film casting process had been the topic of a large number of investigations within the last decades.[1–22] Besides steady state analyses, the so-called draw resonance phenomenon is in the center of many studies since it was first observed by Christensen[23] and Miller.[24] Exceeding a critical value of the draw ratio, i.e., the ratio of the outlet to the inlet velocity, it leads to oscillations in both flow velocity and geometry of the sheet, finally ending up with minor quality of the endproduct and a possible breakdown of the process.

A comprehensive review of the various studies on draw resonance in film casting is given in Chapter 10 of the book edited by Hatzikiriakos and Migler.[25] In most cases, a linear stability analysis is used to detect the onset of draw resonance, which was applied for the first time by Yeow.[1] He used a one-dimensional Newtonian model, derived under the assumption of constant film width and letting the thickness vary only in stretching direction. This model had been extended afterwards to viscoelastic fluids,[3,6] non-isothermal effects,[2,12] and additional external forces like gravity and inertia.[11,14] Bechert, Schubert, and Scheid[14] introduced the dimensionless fluidity and inlet velocity as control parameters and proposed a stability map for these two parameters. Explicit empirical expressions for the critical draw ratio were presented and for the first time, a region of unconditional stability, within

a)Author to whom correspondence should be addressed. Electronic mail: mathias.bechert@fau.de

which no draw resonance and thus no critical draw ratio exists, was revealed. Inertia is supposed to be the cause for this effect, even though no underlying physical mechanism has been found yet.

A major drawback of the above-mentioned one-dimensional model is its inability to reproduce the experimentally known neck-in effect, which describes the reduction of width along stretching direction. It is the result of an interplay between uniaxial extensional deformation near the edges and planar extensional deformation around the central streamline.[15] In purely uniaxial elongation, the width of a fluid element is reduced due to the stress-free edges. In purely planar elongation, the width is fixed to a constant value, resulting in purely parallel streamlines. Two-dimensional models accounting for the neck-in effect have been presented and analyzed with respect to steady state dynamics in the case of isothermal[4] and non-isothermal[8] processing conditions for Newtonian fluids as well as for viscoelastic fluids.[16] A three-dimensional model was developed by Sakaki *et al.*[17] All of these works do not account for the time-dependent dynamics, which makes it impossible to analyze the draw resonance behavior.

Silagy, Demay, and Agassant[18] were the first to present a study on draw resonance in film casting using a model with finite width. Proposing *a priori* a linear transverse velocity profile, they reduced a two-dimensional model to a one-dimensional model with varying width. This made it possible to both describe the neck-in effect and to perform a linear stability analysis with respect to the aspect ratio, i.e., the ratio of the initial film half-width to the film length, and, in the case of viscoelastic fluids, the Deborah number. The neck-in effect turned out to have a stabilizing influence, and an optimal aspect ratio corresponding to maximum stability could be determined. Later, they compared these results with those of a two-dimensional model.[19] In the latter case, however, the stability could only be investigated in terms of full transient solutions. The results were in qualitative agreement with the ones of the one-dimensional model, with only a small shift of the position of the stability maximum. Kim *et al.*[20] later calculated the transient solutions of a two-dimensional viscoelastic model, which was extended afterwards by Shin *et al.*[21]

Recently, Ahmed and Khayat[22] presented a three-dimensional stability analysis of film casting. While they accounted for time dependent perturbations in all three spatial directions, the steady state was reduced to a one-dimensional setup with constant width, neglecting the neck-in effect. The influence of inertia and gravity on the stability behavior was examined. It is stated that, analogue to one-dimensional perturbations, both inertia and gravity have a stabilizing effect and that this effect is even more pronounced if three-dimensional perturbations are present. They also discussed the stability mechanism of inertia and gravity by applying the stability criterion of Kim *et al.*,[26] which is described in more detail below. Both gravity and inertia appear to influence the wave travelling times appearing within the criterion in favor of stability.

The results of Silagy, Demay, and Agassant[18] show that the effect of finite film width is not negligible for realistic film geometries. Additionally, it had been demonstrated by various authors[11,14,22] that both inertia and gravity may have a big influence on the stability behavior. However, no stability analysis including both finite width and additional forces except viscous ones exists up to now. The aim of this paper is to close this gap and to present an investigation of the draw resonance behavior of a finite width film casting process influenced by the effects of gravity and inertia.

As an alternative to linear stability analysis and non-linear transient solutions, Kim's criterion,[26] which is a refinement of the stability criterion of Hyun,[27] can be used to determine the critical draw ratio. Derived by a reformulation of the hydrodynamic equations, it correlates the onset of draw resonance to the travelling times of various perturbation waves, which are moving along the axial direction, and the oscillation period. The criterion was verified for viscoelastic fluids as well[28–30] and thus accepted as a good estimator for critical parameter values. In the case of stable processing conditions, it can be written as

$$(t_L)_1 + (t_L)_2 + T/2 > (\theta_L)_1 + (\theta_L)_2, \tag{1}$$

where $(\theta_L)_1$ and $(\theta_L)_2$ are the travelling times of maximum- and, respectively, minimum-thickness waves, $(t_L)_1$ and $(t_L)_2$ are the corresponding travelling times of a unity-throughput wave, and T is the period of oscillation. At criticality the equality holds in Eq. (1) and the expression can be simplified to

$$2t_L + T/2 = 2\theta_L. \tag{2}$$

Jung, Choi, and Hyun[31] published an approximation of this criterion, which involves only the unity-throughput wave travelling time and the fluid residence time τ_L, together with the time shift Δt_h between the force and the thickness oscillations at the outlet. It has the following form in the case of stable conditions:

$$2t_L + \Delta t_h > \tau_L. \tag{3}$$

There was good agreement to previous results for Newtonian and Maxwell fluids. Scheid *et al.*[12] have applied both Kim's and Jung's criteria to the case of non-isothermal film casting. They discovered that while Kim's criterion remains valid, an additional time difference needs to be introduced to Jung's approximative criterion in order to fulfill the condition at criticality. In this paper, we will enhance the results of Ahmed and Khayat[22] by checking the applicability of Jung's criterion in the presence of inertia and gravity and additionally test both criteria for the case of finite width, which has not been done before.

The paper is structured as follows. The model equations are derived in Section II and the control parameters fluidity, inlet velocity, and aspect ratio are introduced. At the end of the derivation, the local Trouton ratio is defined. Section III first gives a short description of the linear stability method and the continuation algorithm used. Afterwards, the local Trouton ratio is used to separate the space of control parameters into regions of purely planar or purely uniaxial elongation deformation and into a region where both elongation types superimpose. Stability maps of the parameter space are shown in Section IV. The transition to the unconditional stable regime is discussed and analyzed with respect to the parameter values. In Section V, the cases of negligible gravity and negligible inertia are investigated separately using the so-called viscous-inertia and viscous-gravity models, as it turns out that these special cases cover a large part of the practical relevant parameter space. The physical mechanisms underlying the stabilizing effects of inertia, gravity, and neck-in are discussed in Section VI, including an explanation for the unconditional stability caused by inertia. Finally, we apply the criteria of Kim *et al.*[26] and Jung, Choi, and Hyun[31] and test their applicability for our model in Section VII. The paper is concluded in Section VIII.

II. MODEL EQUATIONS

We extend the one-dimensional model introduced by Silagy, Demay, and Agassant[18] to include inertia and gravity. Fig. 1 depicts a three-dimensional sheet which is stretched along the x-axis by prescribing the velocity at the outlet, with z pointing in the width direction. The sheet is defined by the thickness h, the length L, the lateral boundary at $z = \ell(x,t)$, and the velocity field $\mathbf{v} = (u,w)$ with the axial velocity u and the transverse velocity w. The initial film thickness and half-width are denoted, respectively, h_0 and ℓ_0. The fluid speeds at the inlet and at the outlet are noted, respectively, u_0 and $u_0 Dr$, with Dr being the so-called draw ratio. Following the common nomenclature, we introduce the film parameter $\varepsilon = h_0/L$ and the aspect ratio $a = \ell_0/L$.[35] Considering $\varepsilon \ll 1$, i.e., the so-called membrane approximation, the velocity field and the width do not change across the thickness at leading order. The system can then be described by the depth-averaged continuity and momentum equations,

$$\partial_t h + \boldsymbol{\nabla} \cdot (h\mathbf{v}) = 0, \tag{4a}$$

$$\rho h(\partial_t \mathbf{v} + (\mathbf{v} \cdot \boldsymbol{\nabla})\mathbf{v}) = \boldsymbol{\nabla} \cdot (h\boldsymbol{\sigma}) + \rho g h \mathbf{e_x}, \tag{4b}$$

where ρ is the density of the material, assumed to be constant, g is the acceleration of gravity, $\boldsymbol{\sigma}$ is the stress tensor, $\boldsymbol{\nabla} = (\partial_x, \partial_z)$, $\mathbf{e_x} = (1,0)$, and t denotes the time.

The following transformations, also presented in our previous work[14] but extended here for the transverse direction, are used to obtain dimensionless variables: $x \to Lx$, $z \to \ell_0 z$, $u \to \sqrt{gL}u$, $w \to \sqrt{gL}w$, $h \to h_0 h$, $\ell \to \ell_0 \ell$, and $t \to \sqrt{L/g}\, t$. The stress tensor is scaled by $\eta\sqrt{g/L}$, η being the constant dynamical viscosity of the material. The two dimensionless parameters in this scaling are the fluidity F, defined by[36]

$$F = \frac{\sqrt{gL^3}\rho}{\eta}, \tag{5}$$

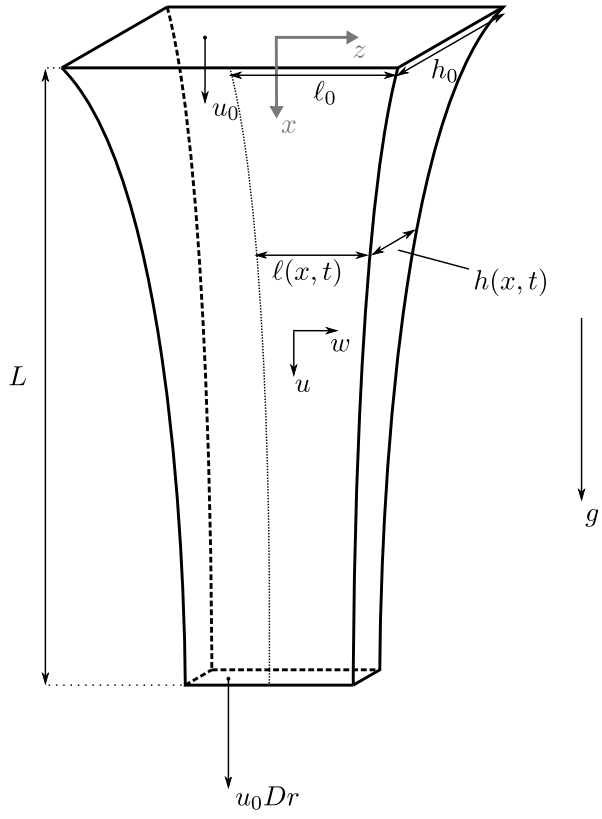

FIG. 1. Sketch of the film casting process.

and the dimensionless inlet velocity Q, defined by

$$Q = \frac{u_0}{\sqrt{gL}}. \tag{6}$$

The boundary conditions at the inlet and at the outlet are

$$h(0,t) = \ell(0,t) = 1, \tag{7a}$$
$$u(0,t) = Q, \tag{7b}$$
$$u(1,t) = QDr. \tag{7c}$$

The velocity scale $\sqrt{gL}$ corresponds to the velocity of a fluid particle falling along the length L under gravity. If F becomes zero, i.e., both inertia and gravity are neglected, Q can take any value above zero, as it can be scaled out in the equations. In these cases, we have set Q to unity throughout the paper. In most works, a slightly different scaling is applied and u is scaled by the initial velocity u_0, leading to the Reynolds number Re and the Froude number Fr instead of F and Q. The transformation rule, however, is straightforward, as $Re = FQ$, $Re/Fr = F/Q$ and boundary conditions (7) change to

$$h(0,t) = \ell(0,t) = 1, \tag{8a}$$
$$u(0,t) = 1, \tag{8b}$$
$$u(1,t) = Dr. \tag{8c}$$

The advantage of the present scaling is that the practical parameters, namely, the viscosity and the inlet velocity, are separately adjustable. Nevertheless, we will switch to the other scaling whenever inertia or gravity is neglected, i.e., in Sections V–VII, as in these cases only one control parameter, $Re/Fr = F/Q$ or, respectively, $Re = FQ$, is needed.

Following Silagy, Demay, and Agassant[18] we use the ansatz of a linear transverse velocity,

$$w = w_\ell(x,t)\frac{z}{\ell(x,t)}, \tag{9}$$

and let the axial velocity u and the thickness h be dependent on x and t only. This enables the construction of a one-dimensional model still accounting for the neck-in effect. The Newtonian constitutive equations for an extensional flow, following the membrane approximation, can then be written as[13]

$$\sigma_{xx} = 4\partial_x u + \frac{2w_\ell}{a\ell}, \tag{10a}$$

$$\sigma_{zz} = 2\partial_x u + \frac{4w_\ell}{a\ell}, \tag{10b}$$

$$\sigma_{xz} = z\partial_x\left(\frac{w_\ell}{\ell}\right). \tag{10c}$$

At the edge $z = \ell(x,t)$, the kinematic condition and the stress balance are given by

$$a(\partial_t\ell + u\partial_x\ell) = w_\ell, \tag{11a}$$

$$\mathbf{n}\cdot\boldsymbol{\sigma}|_\ell = 0, \tag{11b}$$

with the normal vector $\mathbf{n} = (-a\partial_x\ell, 1)/n$ and $n = (1 + (a\partial_x\ell)^2)^{1/2}$. Manipulating (11b) yields

$$\sigma_{zz}|_\ell = (a\partial_x\ell)^2\sigma_{xx}|_\ell. \tag{12}$$

As a result of the linear ansatz for w, σ_{xx} and σ_{zz} are independent of z and equality (12) is true over the whole domain. Together with Eqs. (10a) and (10b), we can derive the constitutive equation

$$\sigma_{xx} = Tr(x,t)\partial_x u, \tag{13}$$

$$\text{with } Tr(x,t) = \frac{6}{2-(a\partial_x\ell)^2}$$

being the *local Trouton ratio*. In the case of slender fiber spinning, i.e., purely uniaxial elongation corresponding to the limit of $a \to 2\varepsilon$, $Tr = 3$. In the case of infinite width film casting, i.e., purely planar elongation corresponding to the limit of $a \to \infty$ and $\partial_x\ell \to 0$ simultaneously, the expression $(a\partial_x\ell)^2$ can be determined by combining (12) and (10), yielding $(a\partial_x\ell)^2 \to 1/2$ and $Tr = 4$. In the case of finite width film casting, both planar and uniaxial elongation will be present and the Trouton ratio is a non-constant quantity between 3 and 4. For the sake of clarity, the two limits mentioned above will be referred to the *uniaxial limit* and to the *planar limit* in the rest of the paper.

Integrating over the entire width and using boundary conditions (11), continuity and momentum equations (4) become

$$\partial_t(\ell h) + \partial_x(\ell h u) = 0, \tag{14a}$$

$$F h\ell(\partial_t u + u\partial_x u) = F\cancel{g}h\ell + \partial_x(h\ell\sigma_{xx}). \tag{14b}$$

Finally, kinematic condition (11a) can be rewritten with the help of Eqs. (10a) and (13),

$$\partial_t\ell + u\partial_x\ell + \frac{\ell}{2}\partial_x u(4 - Tr) = 0. \tag{15}$$

Though we consider the fiber limit $a \to 2\varepsilon$, one has to be aware that our model is rather inappropriate for fiber application, as we are neglecting surface tension, which is an assumption only valid if a is at least one order of magnitude larger than ε. With the range of practical values for a lying between 10^{-1} and 10^2, $a \gg \varepsilon$ is usually verified. Considering the limit of $a \to 2\varepsilon$ is just for mathematical completeness.

III. LINEAR STABILITY ANALYSIS AND IDENTIFICATION OF 2D REGIME

A. Linear stability analysis

The system of PDEs given by Eqs. (13)-(15) is analyzed by common methods of linear stability theory. The four unknowns u, h, ℓ, and σ_{xx} are approximated with the perturbation ansatz

$$u(x,t) = u_s(x)\left(1 + U(x)e^{\lambda t}\right), \tag{16a}$$

$$h(x,t) = h_s(x)\left(1 + H(x)e^{\lambda t}\right), \tag{16b}$$

$$\ell(x,t) = \ell_s(x)\left(1 + L(x)e^{\lambda t}\right), \tag{16c}$$

$$\sigma_{xx}(x,t) = \sigma_{xx_s}(x)\left(1 + \Sigma(x)e^{\lambda t}\right), \tag{16d}$$

where the subscript s denotes the steady-state solutions, U, H, L, and Σ are the complex spatial modes of the perturbation, all assumed to be much smaller than unity and $\lambda = \lambda_R + i\lambda_I$ is the complex eigenvalue, with growth rate λ_R and oscillation frequency λ_I. The steady states are obtained by solving (13)-(15) with $\partial_t \to 0$, whereas (16) is plugged into (13)-(15), which are then linearized, to get the perturbation equations,

$$U' = \frac{\sigma_{xx_s}}{6u_s}\left[2(\Sigma - U) - a^2\ell_s'^2\left(\Sigma - U + 2\left(L + \frac{\ell_s}{\ell_s'}L'\right)\right)\right], \tag{17a}$$

$$H' = -\left[L' + U' + \frac{\lambda}{u_s}(H + L)\right], \tag{17b}$$

$$L' = \frac{3u_s}{2a^2\ell_s^2\sigma_{xx_s}}\left[\frac{3u_s(\Sigma - U + 2L)}{\sqrt{9u_s^2 + 2a^2\ell_s^2\sigma_{xx_s}^2}} - (\Sigma - U + 2L)\right] + \frac{L(\sigma_{xx_s} - 3\lambda)}{\sqrt{9u_s^2 + 2a^2\ell_s^2\sigma_{xx_s}^2}}, \tag{17c}$$

$$\Sigma' = \frac{F}{\sigma_{xx_s}}\left[\Sigma + u_s(\lambda U + (u_sU)' - (\Sigma - U)u_s')\right] - (H' + L'), \tag{17d}$$

where the prime denotes the derivative with respect to x.

The boundary conditions for the steady states are given by (7). For the perturbations, they have the following form:

$$U(0) = U(1) = H(0) = L(0) = 0, \tag{18a}$$

$$\Sigma(1) + H(1) + L(1) = C, \tag{18b}$$

where C defines the arbitrary amplitude of the perturbation of the elongational force $h\ell\sigma_{xx}$ at the outlet and is set to 0.1 hereafter. We have chosen to fix the amplitude of the force perturbation at the outlet, as this facilitates the discussion and visualization of the stability mechanisms in Section VI. Nevertheless, this choice is arbitrary since the system of equations for the perturbations is homogeneous, and other boundary conditions, e.g., fixing $\Sigma(0)$, yield the same stability results.

Solutions are calculated using a continuation method via the software AUTO-07P,[32] as described, for instance, in the work of Scheid *et al.*[13] Starting from the known solution for the planar limit including only viscous forces,[33,34] which can be obtained by setting $a \to \infty$, $Q = 1$, and $F = 0$, the neutral stability curve for which $\lambda_R = 0$, $\lambda_I = \lambda_{Ic}$, and $Dr = Dr_c$ is tracked as a continuous branch in the parameter space spanned by $\{F, Q, a\}$, varying one parameter at a time. Additionally, curves of constant or extremal Dr_c are tracked by fixing the aspect ratio a and varying F and Q simultaneously.

B. Identification of 2D regime

Figure 2(a) shows the neutral stability in terms of the critical draw ratio Dr_c for $F = 0$ and $Q = 1$, as presented by Scheid *et al.*[13] In addition, it appears to be useful to analyze the local Trouton ratio defined in (13) at steady state and criticality, Tr_c, at various positions along the centerline (Fig. 2(b)). A smooth transition from $Tr_c = 3$ for $a \ll 1$ to $Tr_c = 4$ for $a \gg 1$ can be observed, in accordance with the physical interpretation of the one-dimensional uniaxial and planar limits. The particular shapes of the curves change along the axial position in a monotonic way, bounded by the Trouton ratio values at the inlet and at the outlet. The transition from 3 to 4 becomes steeper at the outlet compared to the inlet. This can be explained by the reduction of width caused by the casting process, the so-called neck-in, which can be quantified by the neck-in parameter

$$\xi = 1 - \ell|_{x=1}. \tag{19}$$

As ℓ is scaled by ℓ_0, ξ becomes zero if the width remains constant and increases with increasing width reduction, in general, being bounded between zero and unity. The evolution of the neck-in parameter under variation of the aspect ratio is plotted in Fig. 2(c), together with typical streamlines at three different values of the aspect ratio. Starting at very large aspect ratios in the planar regime,

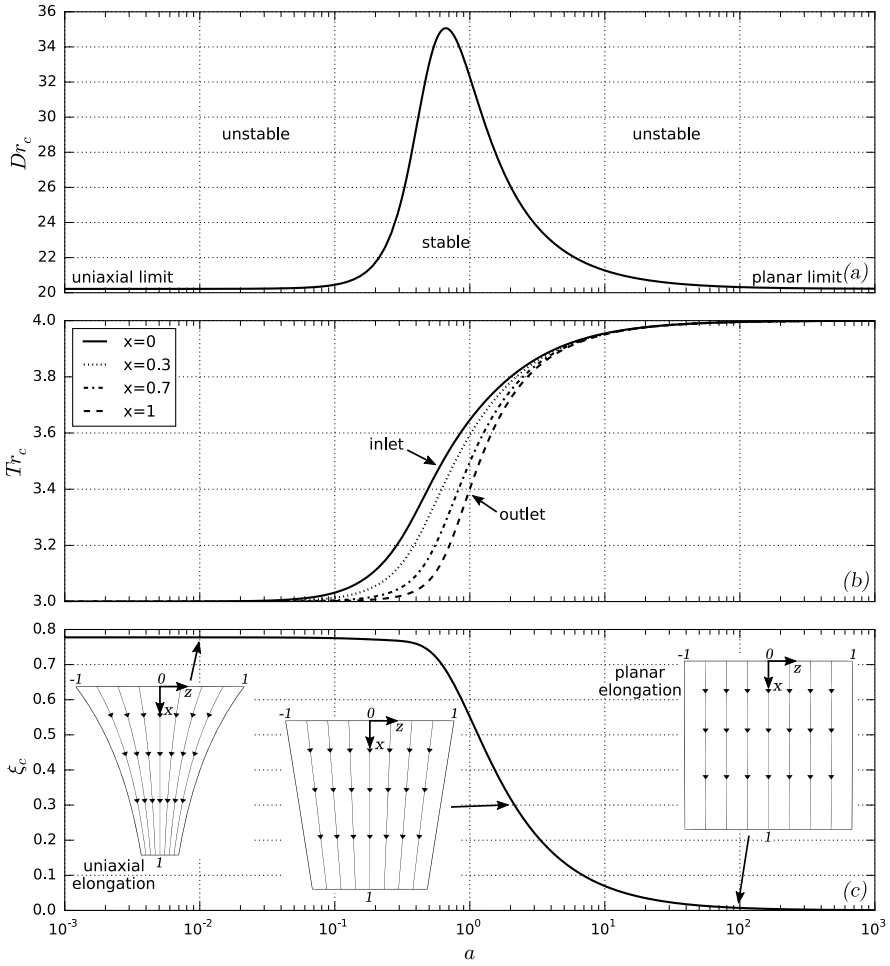

FIG. 2. Influence of the aspect ratio for the fluidity $F = 0$ and the dimensionless inlet velocity $Q = 1$ on (a) the critical draw ratio, (b) the corresponding local Trouton ratio at various x positions, and (c) the corresponding neck-in parameter as defined by (19), together with streamline plots for $a = 0.01$, 2, and 94. The transition of the Trouton ratio curves from the inlet at $x = 0$ to the outlet at $x = 1$ appears to be monotonic.

decreasing the aspect ratio increases the neck-in. As ξ_c increases further, the difference between the Trouton ratios at inlet and at outlet becomes larger, indicating that the ratio of uniaxial to planar elongational deformations increases along x. If a is further reduced towards the uniaxial limit, ξ_c reaches a constant value of $1 - Dr^{-1/2} \approx 0.777$ as $a \to 2\varepsilon$ and $Tr = 3$.

If the Trouton ratio becomes constant, i.e., 3 or 4, the system dynamics reduce to simple uniaxial or, respectively, planar elongation behavior. For $Tr \to 3$, this can be seen in Eq. (15), which then becomes

$$\partial_t \ell + u\partial_x \ell + \frac{1}{2}\ell\partial_x u = 0. \tag{20}$$

The same equation is obtained by replacing h by 2ℓ in (14a), reobtaining purely uniaxial elongation. For $Tr \to 4$, Eq. (15) reduces to $D_t\ell = 0$, with D_t denoting the material time derivative. As the width does not change, we have purely planar elongation in this case. Note that purely uniaxial or purely planar elongation is present if and only if the Trouton ratio is constant, i.e., 3 or, respectively, 4. Consequently, analyzing the Trouton ratio is sufficient for determining whether the finite width of the film has an influence on the stability of the system or not. In the latter case, the one-dimensional models of fiber or, equivalently, film, are fully applicable. From Fig. 2(b), we can infer that the deviation from the constant values of Tr_c is quite small for a outside the interval $[0.1, 10]$. Inversely, for a within this interval the influence of the aspect ratio will change the stability noticeably. In order

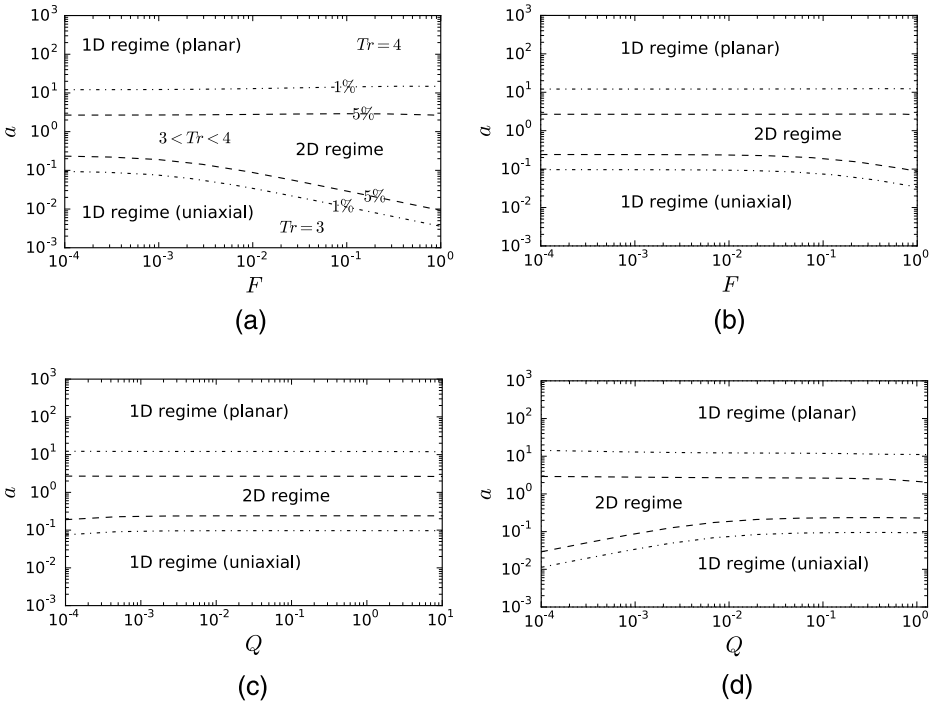

FIG. 3. Dependency of the uniaxial, planar, and two-dimensional regimes on the control parameters F and Q. The inner, dashed lines show the value for a where Tr_c deviates 5% from the constant values, i.e., 4 for the 1D planar regime and 3 for the 1D uniaxial regime, whereas the outer, dashed-dotted lines correspond to a deviation of 1%, as indicated in (a). (a) $Q = 10^{-4}$. (b) $Q = 10^{-2}$. (c) $F = 10^{-3}$. (d) $F = 10^{-1}$.

to analyze the influence of the fluidity F and the inlet velocity Q on the range in which the stability is sensitive to the aspect ratio, Tr_c was calculated with respect to a at the inlet and at the outlet for various combinations of F and Q. The range was then determined as bounded by the values where Tr_c deviates more than 1% or 5% from the constant value of the plateaus. Figure 3 shows the different regimes for constant values of F in the a–Q plane and constant values of Q in the a–F plane. Due to the effect of unconditional stability,[14] the domain of $Q > 1$ could not be analyzed for $F = 0.1$.

The boundary to the 1D planar regime appears to be almost completely independent of the control parameters, being located at $a \approx 10$. The transition to the uniaxial regime happens in some ranges at $a \approx 10^{-1}$; however, if F is quite large and additionally Q is rather small, the two-dimensional regime enlarges towards smaller aspect ratios. In other words, this effect becomes more pronounced if $F/Q = Re/Fr$ is large, revealing gravity as its cause. From Fig. 3, it can be estimated that the effect becomes noticeable for $Re/Fr \gtrsim 10$. As rationalized by Dobroth and Erwin,[15] neck-in is the result of a combination of planar elongation in the middle of the film and uniaxial elongation at the edges. The effect of gravity can then be interpreted as an enforcement of the planar elongation, as a constant force is acting along the axial direction. In the case of small aspect ratios, this may weaken the width reduction as compared to a purely uniaxial elongation. In the case of large aspect ratios however, this effect does not seem to make any difference.

The upper boundary between the two-dimensional and the planar regime is the most relevant one for practical purposes, as it lies within the range of realistic values of aspect ratios. If the aspect ratio exceeds the threshold to the planar regime, the stability analysis presented in our previous work[14] is fully applicable and no neck-in effect has to be taken into account.

IV. STABILITY MAPS

Figure 4(a) shows the critical draw ratio Dr_c vs. the fluidity F for $a = 1$ and $Q = 1$. Every parameter combination $\{Dr, F\}$ below this curve corresponds to stable processing conditions,

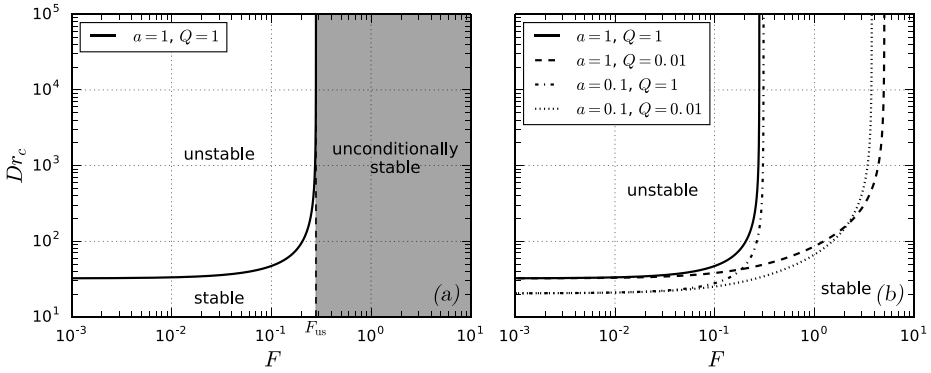

FIG. 4. (a) Neutral stability curve Dr_c vs. F for $a = 1$ and $Q = 1$. Draw ratios below the line correspond to stable parameter combinations, while values above lead to an unstable process. As the curve diverges at $F = F_{us}$, there is no draw resonance for any value of Dr if $F > F_{us}$. (b) Neutral stability curves for various parameter combinations of a and Q. The qualitative shape of the curves remains similar.

while the combinations above the curve lead to draw resonance. As the curve diverges at F_{us}, no draw resonance occurs for $F > F_{us}$ independent of the critical draw ratio, i.e., the system is unconditionally stable. This effect was described in our previous work[14] and is caused by inertia, as it will be discussed in Section VI. Figure 4(b) depicts neutral stability curves for various parameter combinations of a and Q, in order to visualize the similarity of the shapes. The transition point to unconditional stability, F_{us}, can be obtained by fitting the data with a diverging function around the region of divergence.[14] As a result, Fig. 5 shows the threshold parameter F_{us} with respect to Q for various values of a together with the limiting cases of $a \to 2\varepsilon$ and $a \to \infty$. While the curves all exhibit the same trend for $Q > 0.1$, this is not the case for smaller values of Q. Especially for $a = 0.1$, F_{us} decreases strongly with decreasing Q, enlarging the region of unconditional stability. Thus, especially for small Q and large F, or in other words for large values of Re/Fr and thus due to gravity, an aspect ratio around $a \approx 0.1$ has a strongly stabilizing effect.

It can be seen that for $Q > 0.1$, the limit cases of planar and uniaxial elongations are approached for $a \gtrsim 10$ and $a \lesssim 0.1$. For $Q < 0.1$ however, only the planar limit is recovered for $a \gtrsim 10$, while the uniaxial limit is finally reached for $a \lesssim 0.001$. This coincides with the results displayed in Fig. 3, which show that the range of aspect ratios where the finite width has an influence on the stability enlarges towards smaller a if F is large and Q is small. Note that in Fig. 5(a), the curves for different

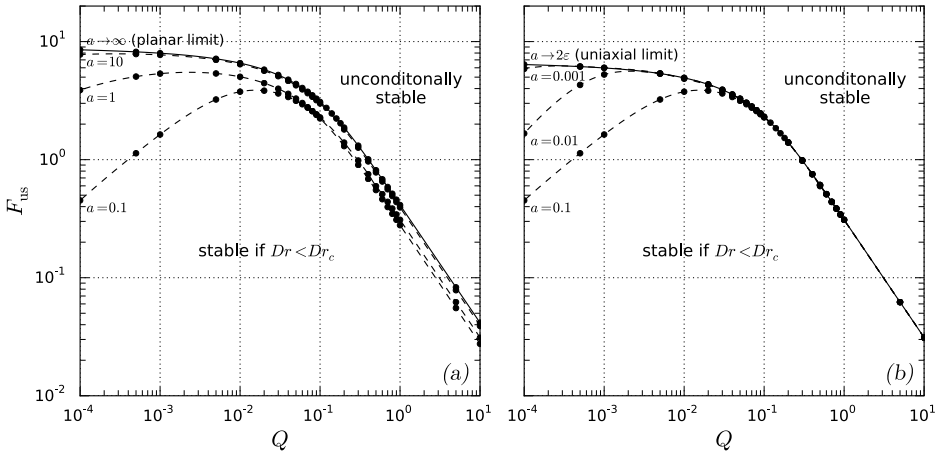

FIG. 5. Threshold values of F for aspect ratios $a = 0.001, 0.01, 0.1, 1, 10$ and the limiting cases $a \to 2\varepsilon$ and $a \to \infty$. For values of F above this curve the system is unconditionally stable. The points correspond to values determined using the neutral stability curves and the lines are approximating splines. Two plots (a) and (b) have been made for clarity.

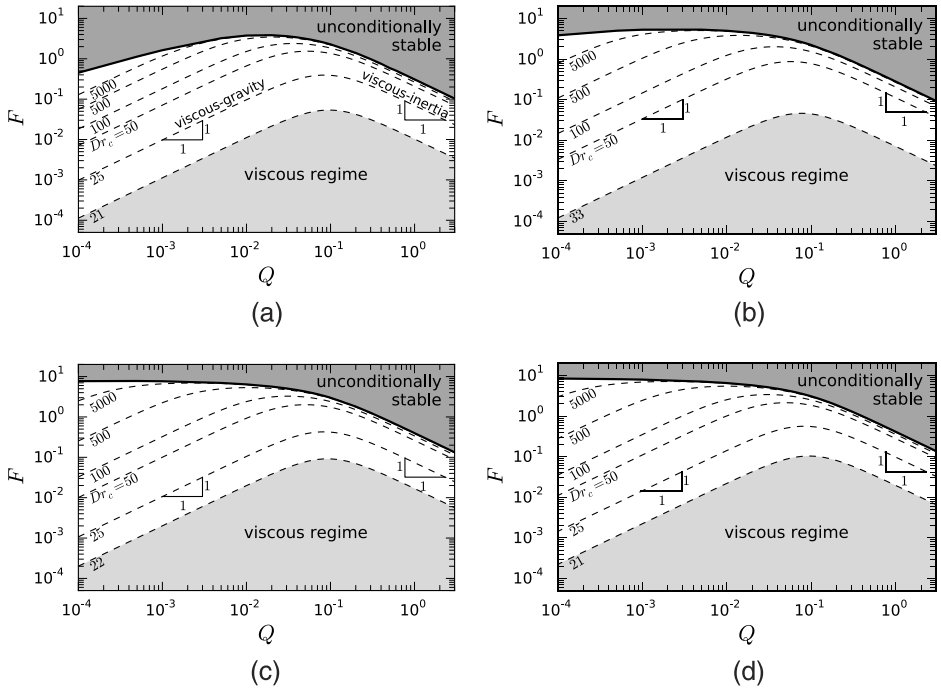

FIG. 6. Stability maps for aspect ratios $a = 0.1$, 1, 10 and in the limit of $a \to \infty$. The dashed lines correspond to parameter sets of constant critical draw ratio. The thick line shows the transition to the unconditionally stable regime (dark shaded). In the light shaded region only viscous effects contribute to the stability of the system. Most of the time, the lines of constant Dr_c show either $F \propto Q$ or $F \propto 1/Q$, indicating that viscous and gravity or, respectively, viscous and inertia effects dominate the stability behavior. (a) $a = 0.1$. (b) $a = 1$. (c) $a = 10$. (d) $a \to \infty$.

values of a can cross over each other, such that the minimum value of F_{us} is a function of both a and Q. As we will show in Section VI, the effect of unconditional stability is influenced by other stabilizing effects, such as gravity. Additionally, as it will be shown in Section V B, the value of a at which Dr_c is maximum decreases with increasing F/Q, leading to the observed dependency of F_{us} on a and Q.

In order to give an overview of the complete stability behavior of the system, Fig. 6 shows stability maps for various values of the aspect ratio. These maps visualize the lines of constant Dr_c in the F–Q space, together with the transition to the regime of unconditional stability. The region below the lowest isoline corresponds to parameter combinations with almost constant Dr_c, i.e., the viscous regime where neither gravity nor inertia has an effect on the stability. Due to the stabilizing effect of the neck-in, which is visualized in Fig. 2(a) for the viscous regime, i.e., $F = 0$ and $Q = 1$, the absolute value of the critical draw ratio changes for different aspect ratios. The qualitative influence of the fluidity F and the inlet velocity Q however remains similar for most of the parameter space. Apart from the viscous regime and the one of unconditional stability, the lines of constant Dr_c reveal mostly either a proportionality or a reciprocal correlation between F and Q, as shown by the 1-to-1 slope. This means that within these regions the critical draw ratio depends on F/Q in the former case and on FQ in the latter case only. Since $F/Q = Re/Fr$ and $FQ = Re$, as already mentioned above, these regions correspond to the *viscous-gravity* and, respectively, *viscous-inertia* regimes, which means that inertia or gravity does not influence the stability behavior. For the case of $a \to \infty$, this separation into different regimes was discussed in our previous work[14] together with empirical correlations between Dr_c, F, and Q.[37] For the case of finite width, we will not try to find similar correlations, as the parameter space including the aspect ratio is too large to do an analogue analysis. However, the stability maps show that the cases of a viscous-inertia model and a viscous-gravity model are of great importance, as they cover most of the practical parameter space. Therefore, it is worth to study their behavior separately, which is done in Section V.

V. VISCOUS-INERTIA AND VISCOUS-GRAVITY REGIMES

A. Viscous-inertia regime

From the stability maps of Fig. 6, it can be inferred that gravity effects can be neglected in good approximation if $Q \gtrsim 0.1$. In this case there are, besides Dr, only two effective control parameters left, namely, the Reynolds number $Re = FQ$ and the aspect ratio a. The model equations remain almost identical except for Eq. (14b), where the first term on the right-hand side is dropped. For this and Secs. VI and VII, boundary conditions (8) are used instead of (7). A linear stability analysis with respect to the two control parameters was performed and the results are shown in Fig. 7. Figure 7(a) shows the influence of the aspect ratio on the critical draw ratio for various values of Re. The stabilizing effect of inertia can be seen for all curves, which are shifted to higher Dr_c compared to the curve of the purely viscous model for $Re = 0$. Additionally, the height of the maximum at $a = 0.66$, labeled by "V" in Fig. 7, is increased with increasing Re, finally leading to an opening of the curves and revealing a region of unconditional stability within the domain of a. Note that the critical Reynolds number, above which this region appears, lies below the value of 0.4 determined in our previous work[14] for the planar limit. This can be seen as well in Fig. 7(b), which shows the isolines of Dr_c in the Re–a plane. The threshold line to unconditional stability shows a minimum at $a = 0.50$, labeled by "C", which makes the transition from the uniaxial to the planar limit non-monotonic, in contrast to the transition of the local Trouton ratio in Fig. 2. The point of maximum stability moves to lower aspect ratios as the Reynolds number becomes larger. However, the total difference is rather small, from $a = 0.66$ to $a = 0.50$. The isolines of Dr_c in Fig. 7(b) reach different plateau values for small and large values of a. This is due to the fact that the uniaxial and planar Trouton ratios are not identical, leading to a ratio of 3/4 between the plateau values.

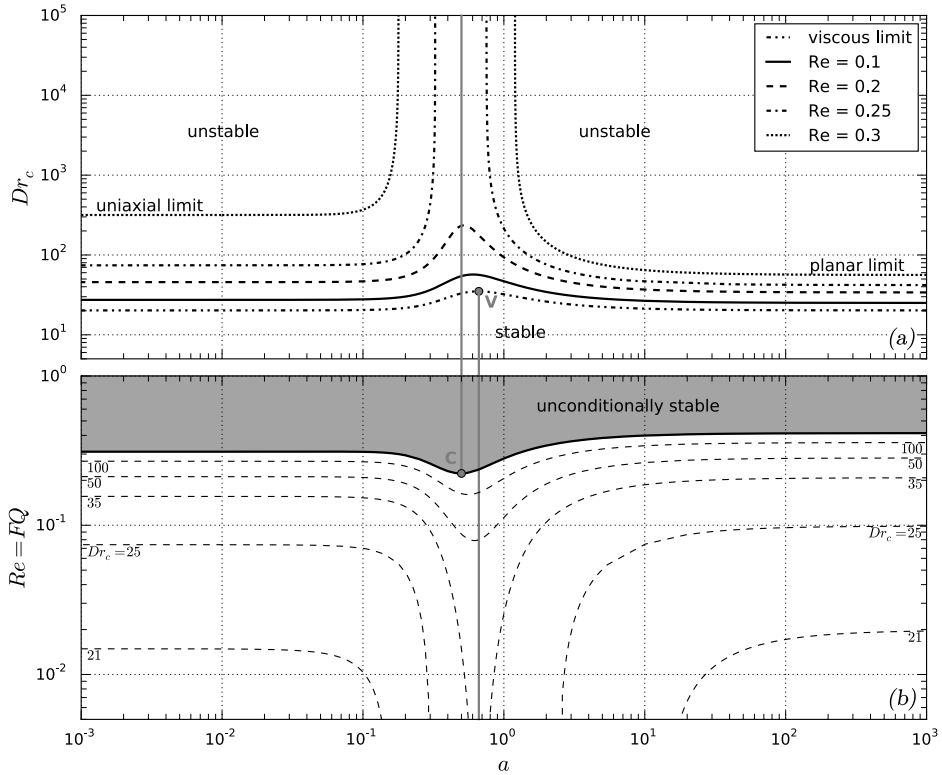

FIG. 7. (a) Stability curves Dr_c vs. a for various values of Re and (b) stability map with isolines for $Dr_c = 21, 25, 35, 50, 100$, both in the viscous-inertia regime. For $Re = 0$, label "V" indicates the largest value of Dr_c, equal to 35.1 and located at $a = 0.66$, while label "C" refers to the minimum value of $Re = 0.22$, above which unconditional stability is possible, occurring at $a = 0.50$. The entire region of unconditional stability is shaded grey in (b).

B. Viscous-gravity regime

Besides the viscous-inertia regime, the viscous-gravity regime also covers a wide region in the parameter space, as shown in Fig. 6. The viscous-gravity model becomes applicable when $Q \lesssim 0.1$ and F is not too close to the critical value. The corresponding equation is obtained by setting the left-hand side in Eq. (14b) to zero. Consequently, the ratio of Reynolds to Froude number, $Re/Fr = F/Q$, is besides a and Dr the remaining control parameter. Results of the linear stability analysis are visualized in Fig. 8.

Analogue to Fig. 7, Fig. 8(a) shows curves of constant ratio of Re/Fr in the Dr_c–a plane and Fig. 8(b) shows isolines of Dr_c in the Re/Fr–a plane. In contrast to the viscous-inertia regime no unconditional stability was detected for any parameter combination, as we found in the planar limit[14] and once again indicating that inertia is responsible for the unconditional stability behavior. Still, gravity enhances the stability of the system, as the Dr_c vs. a curves are shifted towards larger Dr_c with increasing Re/Fr. While the position of the maximum is almost invariant on Re for the viscous-inertia model, it is shifted clearly towards smaller aspect ratios by the effect of gravity. For this reason, the locus of the maximum was calculated with respect to Re/Fr. Figure 9 shows the maximum critical draw ratio $Dr_c^{\max}$, its relative value with respect to the critical draw ratio in the planar limit ($a \to \infty$), and the corresponding value of the aspect ratio, denoted $a_{\max}$. The maximum critical draw ratio increases clearly with increasing Re/Fr (see Fig. 9(a)). Note that this is not solely due to the same effect as for the one-dimensional limit values, as the ratio of the maximum critical draw ratio to the critical draw ratio in the planar limit increases as well (see Fig. 9(b)). This means that gravity does not only enhance stability for all aspect ratios, but additionally enforces the stabilizing effect of neck-in, too. For instance, at $Re/Fr = 10^3$, the value of Dr_c at $a \approx 0.16$ is one order of magnitude higher than the planar limit value. For $Re/Fr = 0$, there is only an amplification factor of 1.7. Figure 9(c) shows that the value of aspect ratio at which maximum stability is reached lies between 0.1 and 0.66, depending on the value of Re/Fr. This changing influence of the aspect

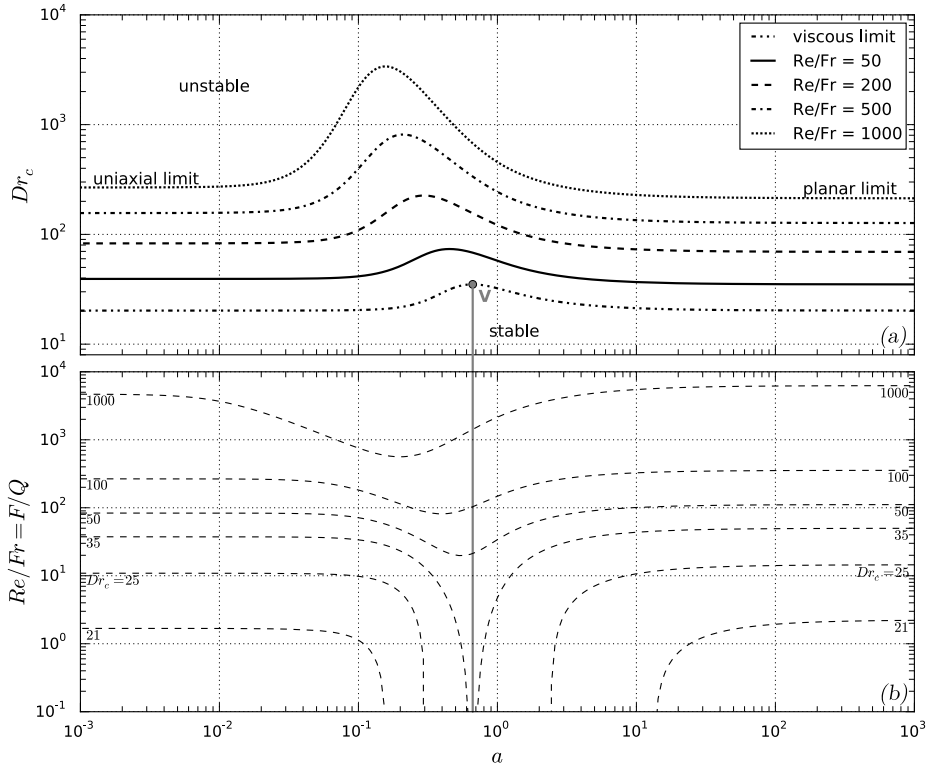

FIG. 8. (a) Stability curves Dr_c vs. a for various values of Re/Fr and (b) stability map with isolines for $Dr_c = 21, 25, 35, 50, 100, 1000$, both in the viscous-gravity regime. For $Re/Fr = 0$, label "V" indicates the largest value of Dr_c, equal to 35.1 and located at $a = 0.66$.

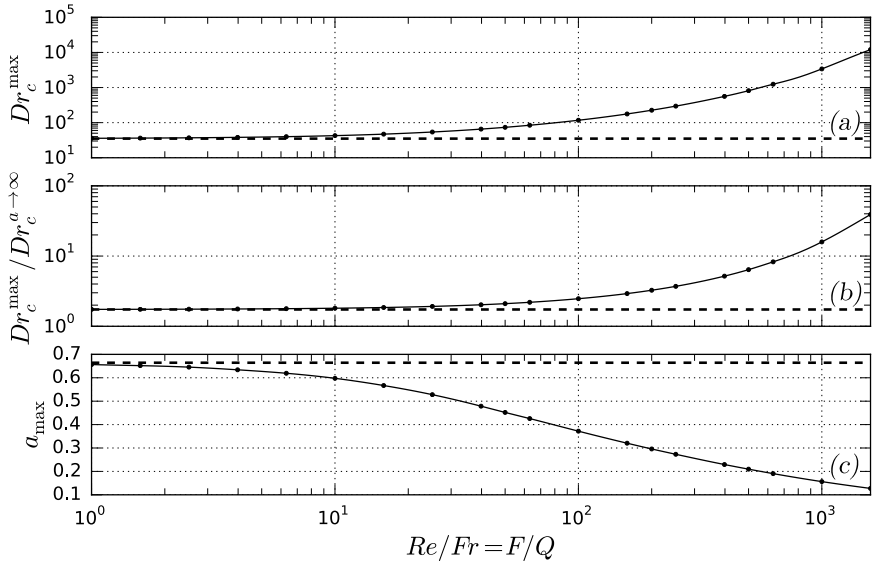

FIG. 9. Visualization of the influence of gravity on the position of the stability maximum (label "V" in Fig. 8). The dots are the calculated values from the neutral stability curves. The continuous lines are approximated splines. The dashed lines indicate the corresponding value for $Re/Fr = 0$, when only viscous forces are present. The maximum critical draw ratio $Dr_c^{\max}$ (a) increases as well as the ratio of the maximum critical draw ratio to the critical draw ratio in the planar limit (b) with increasing gravity effect, i.e., increasing Re/Fr. The aspect ratio $a_{\max}$, at which the maximum is reached, becomes significantly smaller with increasing Re/Fr (c).

ratio on the stability behavior can be correlated with the dependency of the two-dimensional regime on the control parameters, depicted in Fig. 3. As the two-dimensional regime enlarges for large Re/Fr in an asymmetric way, i.e., towards small aspect ratios, the center of this regime moves to smaller aspect ratios as well.

VI. STABILITY MECHANISMS

In the following, the basic principles of the physical mechanisms underlying the stabilizing effect of inertia, gravity, and neck-in are discussed. It is important to understand the general feedback mechanism causing draw resonance, which had been pointed out before by various authors.[12,26] The dimensionless force f acting along the axial direction can be calculated with Eq. (13) as

$$f = Trh\ell\partial_x u. \tag{21}$$

In the absence of gravity and inertia, momentum equation (14b) directly shows that this force is independent of x and depends only on time. In any other case, however, it also depends on the spatial position. Nevertheless, a perturbation of the force at the outlet will influence the gradient of the cross section area at the inlet, which can be seen clearly in the purely viscous case of a constant force, i.e., $F = 0$ and $Q = 1$, from continuity equation (14a), as the time derivative vanishes at the inlet because of boundary conditions (8),

$$(\partial_x(h\ell))\,|_{x=0} = -\frac{f}{Tr|_{x=0}}. \tag{22}$$

For a non-constant force, both intuition and numerical calculations suggest that there exists a similar correlation between the force at the outlet and the change of cross section area at the inlet, even if it cannot be written in such an easy form due to additional phase shifts or other effects. Consequently, a temporary increase of the force leads to a temporary decrease of the cross section area at the inlet. This minimum-cross section wave travels downwards and leads to a minimum of the force at the outlet. Note that the minimum force is reached $\Delta t_{h\ell}$ (or Δt_h in the planar limit) before the minimum cross section area reaches the outlet. Consequently, a decrease of f leads to an increase of $h\ell$ at the inlet, which is again travelling downwards and completing the cycle of draw resonance.

A. Stabilizing mechanisms of inertia and gravity

The stabilizing effect of inertia, which eventually leads to unconditional stability, had already been presented before,[14] though without a concrete explanation of the underlying mechanism. In the following, the underlying principle of the mechanism is demonstrated. In order to keep it as simple as possible and to concentrate on the essential part, we will neglect gravity effects and stay in the planar limit, such that besides the draw ratio, the Reynolds number $Re = FQ$ is the only remaining control parameter. Fig. 10(a) shows steady state velocity profiles for two distinct values of Re but for the same draw ratio ($Dr = 1000$). It can be seen that increasing the Reynolds number lowers the velocity values over the entire domain, leading to a sharp increase near the outlet such that the boundary condition is fulfilled, which has already been reported before.[11] This behavior is caused by the damping effect of inertia, which hinders the equal distribution of the force accelerating the fluid along the x-axis, as shown in Fig. 10(b). While the force is constant in the viscous limit, i.e., for $Re \to 0$, it shows a sharp increase near the outlet if inertia is present. As a result, a large part of the fluid dynamics is governed by a smaller force, i.e., a smaller acceleration, if inertia is increased.

The steady state velocity can be calculated as (see Appendix A)

$$u_s(x) = \frac{c}{(c + Re)e^{-cx/4} - Re}, \tag{23}$$

with $c = c(Re, Dr)$ being a constant which is determined numerically so that the boundary condition at the outlet, $u_s(1) = Dr$, is fulfilled. The force f can then be calculated as

$$f_s(x) = h_s \partial_x u_s = \frac{\partial_x u_s}{u_s} = \frac{c(c + Re)}{4\,(c + Re - e^{cx/4}Re)}. \tag{24}$$

By a rough and simple approximation, the velocity and force profiles can be approached by the viscous limit, where the force remains constant over the axial domain. If we assume the force to be constant with value $f_s(0) = (c + Re)/4$, the velocity profile becomes merely $u_s(x) \approx e^{(c+Re)x/4}$. This "constant force" approximation is also plotted in Fig. 10. From this form, an "effective draw ratio" can be calculated as $Dr^{\text{eff}}(Re, Dr) = e^{(c+Re)/4}$. This effective draw ratio was calculated for various combinations of Re and Dr and compared to 20.218, i.e., the critical value in the purely viscous limit. For a fixed value of Re, the draw ratio at which the corresponding effective draw ratio exceeds 20.218 has then been taken as approximated critical draw ratio $Dr_c(Re)$. This procedure is visualized in Fig. 11. The resulting stability curve is shown in Fig. 12 and compared with the exact numerical solution. The qualitative shapes of the curves coincide perfectly; however, the stabilizing effect of inertia is underestimated. The constant force approximation is rather underestimating the effective draw ratio, too. Consequently the discrepancy of the two stability curves would be even larger, if the approximation is improved. Nevertheless, we can explain with this simple argument why inertia can lead to unconditional stability: If Re is large enough, the effective draw ratio determining the fluid dynamics along the major part of the x-axis is always below a critical value, which can itself be below the true value of draw ratio. Consequently, the draw ratio can become arbitrarily large,[38]

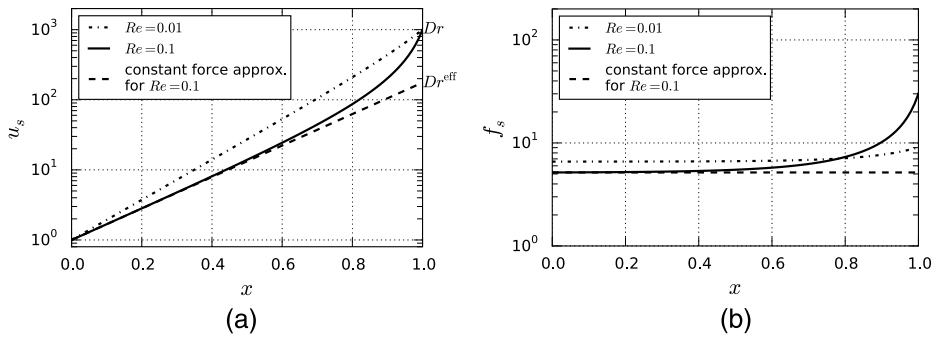

FIG. 10. Steady state profiles of the viscous-inertia model in the planar limit for two different Reynolds numbers as well as the "constant force" approximation, as discussed in the text; $Dr = 1000$. (a) Steady state profiles of the axial velocity. (b) Steady state profiles of the force.

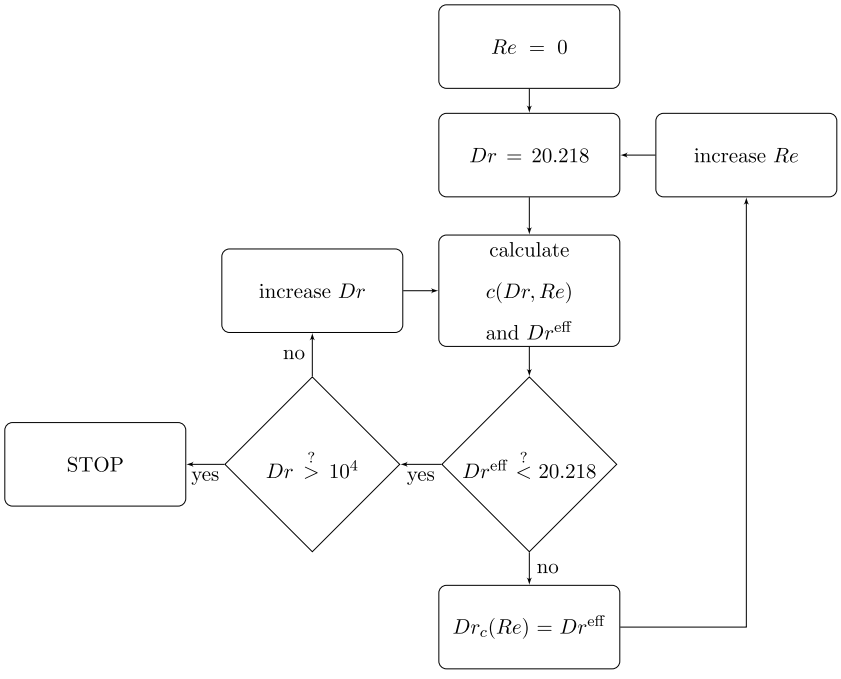

FIG. 11. Flow chart of the algorithm for calculating the approximative stability curve shown in Fig. 12. Due to the convex velocity profile, Dr^{eff} is always equal or below Dr; therefore, Dr can be set to 20.218 as starting value. The calculation ends if a draw ratio equal or above 10^4 is still stable according to the approximative criterion.

as it is not the crucial parameter influencing the draw resonance behavior if inertia forces are high enough. The difference between the approximate and the exact solutions in Fig. 12 is probably due to additional effects which influence the evolution of the perturbation waves in favor of stability, which is shortly described below. However, it is shown here that it is enough to analyze the steady state behavior in order to reproduce the divergent character of the stability curve.

This mechanism also explains why, in presence of inertia and gravity, the threshold value F_{us} decreases with decreasing Q if $Q < 0.1$. The stabilizing effect of gravity, which becomes important in this parameter region, increases the critical draw ratio. Consequently, the damping effect of inertia leads faster to unconditional stability, as the threshold value for the effective draw ratio becomes larger. The same argument explains the minimum of the threshold value for Re at $a = 0.50$ in Fig. 7, as the influence of the aspect ratio shows a stabilizing maximum nearby.

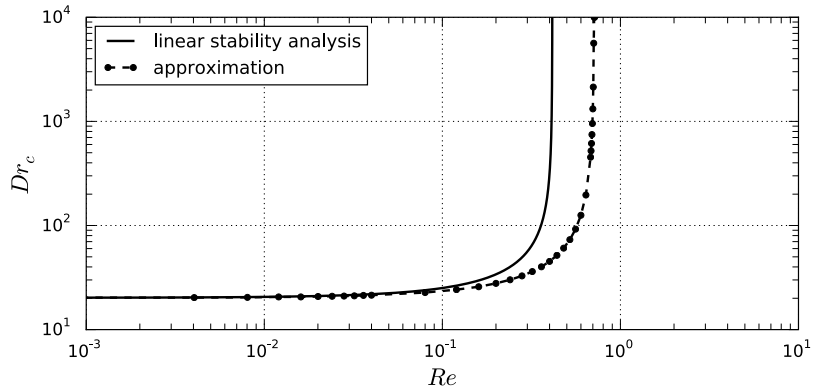

FIG. 12. Comparison of the numerical solution of the linear stability analysis with the approximated stability curve for the viscous-inertia model in the planar limit. The stabilizing effect of inertia is underestimated, but the essential mechanism underlying the unconditional stability is reproduced.

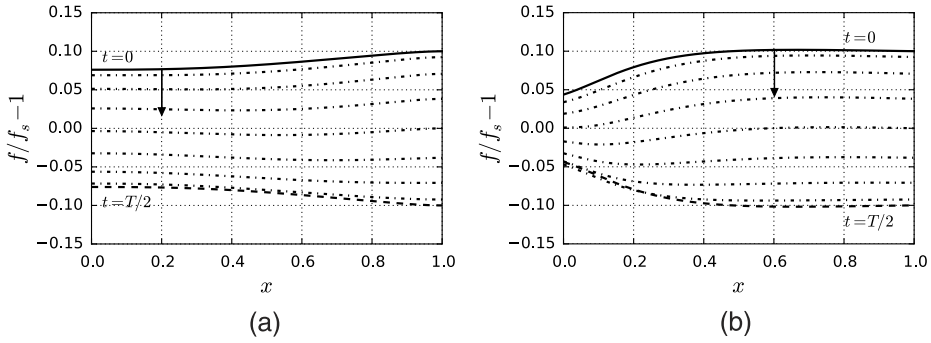

FIG. 13. Force perturbation waves along the x-axis for $Re = 0.3$, neglecting gravity, and $Re/Fr = 100$, neglecting inertia. The thick lines correspond to time $t = 0$, the dashed lines correspond to time $t = T/2$, and the dashed-dotted lines in between correspond to increasing time along the arrow, with incremental step size of $T/16$. (a) $Re = 0.3$ (viscous-inertia regime). (b) $Re/Fr = 100$ (viscous-gravity regime).

Basically, inertia and gravity have a stabilizing effect as they lead to a decreasing amplitude of the force oscillation near the inlet compared to the amplitude at the outlet. This effect can be seen in Fig. 13, which shows the force perturbation wave along the x-axis at several values in time within a half-oscillation period T, for $Re = 0.3$ in the viscous-inertia regime and for $Re/Fr = 100$ in the viscous-gravity regime. Following an initial perturbation at the outlet towards the inlet, the oscillation amplitude decreases with decreasing x, i.e., during travelling to the inlet, if inertia or gravity is present, which damps the feedback mechanism of draw resonance and leads to an increase of stability. The stabilizing effect of gravity is quite intuitive, as the external, additional force acting in axial direction is not affected by the perturbations.

B. Stabilizing mechanism of the neck-in

In order to carve out the stabilizing effect accompanying the neck-in, we will set $F = 0$ for the following. In this case, the force f given by Eq. (21) is constant along the x-axis. In particular, the force at the outlet is equal to the force at the inlet, including the time dependent perturbations. However, in contrast to the planar limit, the Trouton ratio is not constant, which influences the feedback mechanism in the following way. Using Eq. (22), the following relation can be written due to the constant force:

$$(\partial_x (h\ell))^{\text{in}} = -\frac{Tr^{\text{out}}}{Tr^{\text{in}}} h^{\text{out}} \ell^{\text{out}} (\partial_x u)^{\text{out}}, \tag{25}$$

where the superscripts indicate the position at the inlet and outlet. Equation (25) points out that the ratio of the Trouton ratios at the outlet to those at the inlet influences the amplitude of perturbation waves at the inlet (left-hand side) which are caused by perturbations at the outlet (right-hand side). Fig. 14 shows this ratio for the steady state at criticality over the domain of aspect ratios. A minimum occurs at $a \approx 0.58$, close to the stability maximum at $a \approx 0.66$. Consequently, the varying Trouton ratio is the key to the stabilizing mechanism of the neck-in effect, as the geometric difference between the inlet and the outlet leads to a different effect on the cross section area, although the force does not change.

Further investigations (not presented) have shown that the influence of the time dependent perturbative part of the Trouton ratio has only negligible influence on this result. Up to now, we do not have an explanation for the (small) mismatch of the stability maximum and the minimum of the ratio of the Trouton ratios. We believe, however, that the reason for this are one or several other stabilizing effects, which have a maximum impact at values of a in the vicinity of 0.66, and which lead in total to the observed stability maximum. This hypothesis is supported by the results of Section VII B, which reveal that the various calculated travelling times show extremas at slightly different values of the aspect ratio.

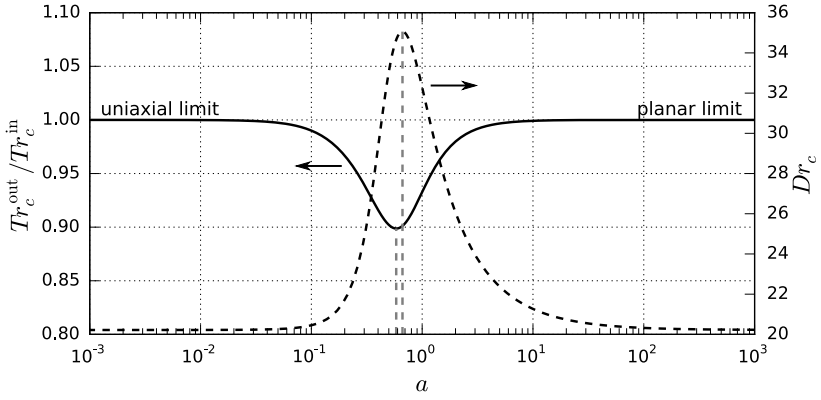

FIG. 14. Plot of the ratio of the steady state Trouton ratios at criticality at the outlet and at the inlet (thick line). Close to the maximum of the critical draw ratio (dashed line) at $a = 0.66$, this ratio shows a minimum at $a = 0.58$.

VII. STABILITY CRITERIA

We will now apply the stability criterion of Kim *et al.*,[26] which is based on exact transient solutions and given by Eq. (2), and the approximative criterion of Jung and Hyun,[28] which is based on steady state solutions and given by Eq. (3), and test their validity in case of inertia and gravity effects and neck-in. In particular, Kim's criterion had already been verified in the planar limit including inertia and gravity by Ahmed and Khayat[22] and will be presented here only for the sake of completeness.

The relevant parameters were calculated in all cases by the following procedures. The fluid residence time τ_L was obtained by numerical integration of $1/u_s$ over the x-domain. The calculation of the unity-throughput[39] wave travelling time t_L is described in Appendix B. The travelling time of a maximum perturbation wave θ_L was computed by numerically tracking the maximum of the sinusoidal perturbation waves at criticality along the x-axis and computing the difference between the time values at the outlet and at the inlet. The time shift Δt_h between the force and the thickness oscillations at the outlet is equal to the complex angle of $H(1)$, as the perturbation of the force at the outlet is defined to be 0.1 according to Eq. (18b) and thus always real.

A. Gravity and inertia (planar limit)

Fig. 15 shows that in the absence of inertia, both Kim's and Jung's criteria are valid over the analyzed domain of F and Q, which can be combined in this case to the single control parameter $Re/Fr = F/Q$. On the other hand, Fig. 16 shows the calculated times in the absence of gravity with respect to $Re = FQ$. While Kim's criterion is still valid, Jung's approximative criterion shows

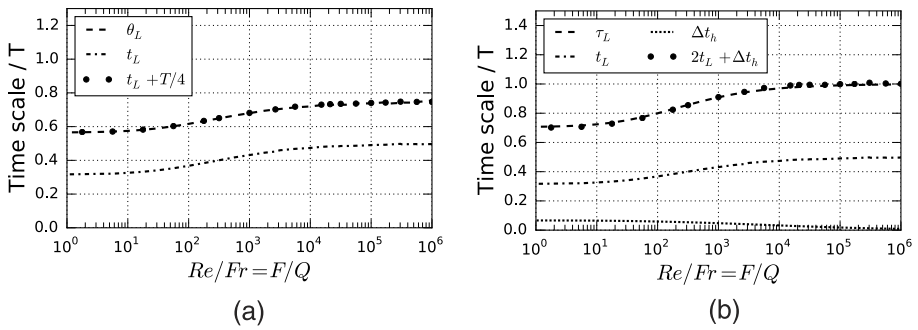

FIG. 15. Comparison of Kim's stability criterion (2) and Jung's approximative stability criterion (3) at criticality for the planar limit in the viscous-gravity regime. The time is scaled with the period T of the oscillation. Only few markers are shown for $t_L + T/4$ and $2t_L + \Delta t_h$ for the sake of readability. (a) Kim's criterion. (b) Jung's criterion.

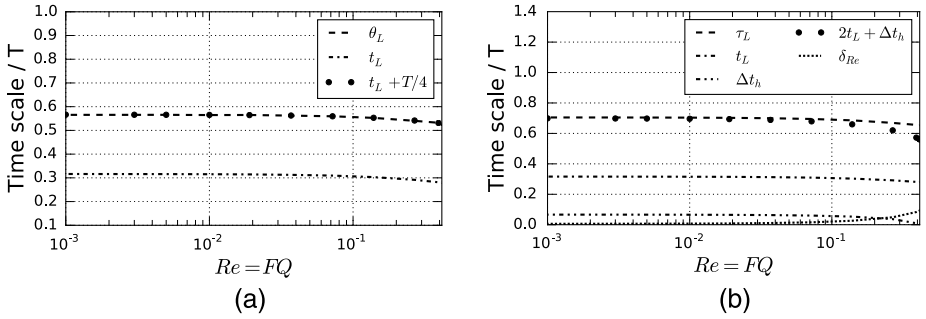

FIG. 16. Comparison of Kim's stability criterion (2) and Jung's approximative stability criterion (3) at criticality for the planar limit in the viscous-inertia regime. The time is scaled with the period T of the oscillation. Only few markers are shown for $t_L + T/4$ and $2t_L + \Delta t_h$ for the sake of readability. (a) Kim's criterion. (b) Jung's criterion.

increasing discrepancies with increasing Reynolds number. Therefore, criterion (3) needs to be modified by an additional time shift δ_{Re}, which is identical to the difference between τ_L and $2t_L + \Delta t_h$ at criticality,

$$2t_L + \Delta t_h + \delta_{Re} > \tau_L. \tag{26}$$

As we are not able to derive an expression for δ_{Re}, Jung's criterion is not useful if inertia is present. Both Figs. 15 and 16 show that Δt_h vanishes for large Re/Fr or Re, respectively, i.e., the thickness and the force oscillations are in phase at the outlet. This effect turned out to be due to the large value of draw ratio at criticality and does not seem to have a major impact on the stability behavior.

B. Finite width (viscous limit)

If the effect of finite width is taken into account, the governing equations change fundamentally and raise the need for an extension of Kim's criterion. Following the derivation of Kim *et al.*,[26] it turns out that the maximum perturbation wave travelling time θ_L cannot be calculated by the thickness perturbation alone anymore, but corresponds to the perturbation of the cross-sectional area, i.e., $h\ell$. Thus θ_L is the travelling time of the maximum of $H + L$. Similarly, the time shift Δt_h is replaced by $\Delta t_{h\ell}$, the time shift between the force and the cross section area oscillations at the outlet.

In the viscous limit, i.e., $F \to 0$ and $Q = 1$, Fig. 17 shows that Kim's criterion remains valid for the finite width model. Jung's criterion, however, shows mismatch around the stabilizing region of a, and an additional δ_a is needed to correct the criterion. Similar to the time shift δ_{Re} induced by inertia, we cannot derive an expression for δ_a. Jung's criterion is motivated solely by empirical observations of the numerical data, which makes it hard to modify or extend it to the finite width

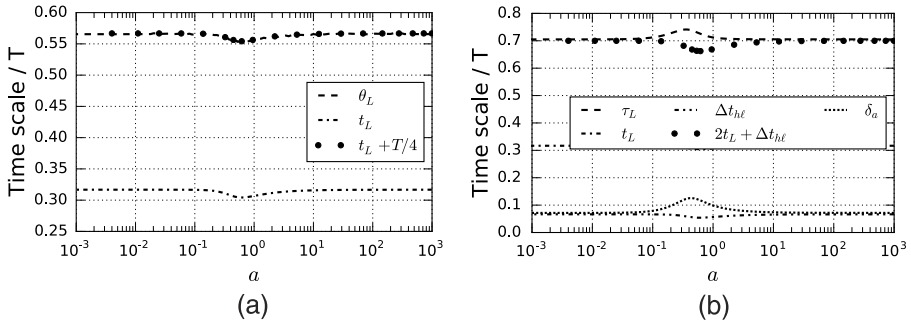

FIG. 17. Comparison of Kim's stability criterion (2) and Jung's approximative stability criterion (3) at criticality for finite width in the purely viscous regime. The time is scaled with the period T of the oscillation. Only few markers are shown for $t_L + T/4$ and $2t_L + \Delta t_{h\ell}$ for the sake of readability. (a) Kim's criterion. (b) Jung's criterion.

model following physical arguments. Consequently, it can only be stated that in the general case of finite film width, Jung's criterion cannot be applied any more. θ_L, t_L, and $\Delta t_{h\ell}$ have minimum values at $a \approx 0.62$, while the fluid residence time τ_L becomes maximum at $a \approx 0.36$. Note that these values are influenced by the scaling with the period T, which is itself dependent on a and has a minimum at $a \approx 0.58$ (not shown).

VIII. SUMMARY AND CONCLUDING REMARKS

We have presented an analysis of the draw resonance instability in Newtonian film casting processes under the influence of gravity and inertia and accounting for the neck-in, a reduction of width along the stretching direction. This effect itself has a stabilizing influence on the process, as Silagy, Demay, and Agassant[18] had shown for a purely viscous model, neglecting gravity and inertia. Besides the three independent, dimensionless control parameters, i.e., the aspect ratio, the fluidity, and the inlet velocity, we introduced the local Trouton ratio, which serves as a measure of the type of elongational deformation, being uniaxial for $Tr = 3$, planar for $Tr = 4$, or a combination of the two for $3 < Tr < 4$.

Analyzing the evolution of the local Trouton ratio with respect to the control parameters made it possible to separate the domain of aspect ratios into a two-dimensional regime, where neck-in influences the stability of the system, and one-dimensional regimes, where either purely planar or purely uniaxial elongation exists and consequently where a one-dimensional model is sufficient. For most parameter combinations, the two-dimensional behavior occurs for aspect ratios within $[0.1, 10]$, but gravity was found to enlarge the two-dimensional regime towards smaller aspect ratios.

Stability maps in the parameter space spanned by the fluidity and the inlet velocity were shown for various values of the aspect ratio, revealing the special cases of viscous-gravity and viscous-inertia models to be valid for most of the practical parameter combinations. The influence of the control parameters on the boundary to unconditional stability was analyzed as well. For small values of inlet velocity and aspect ratios around 0.1, the threshold fluidity is lowered by up to one order of magnitude. Gravity shifts the position of the stability maximum towards smaller aspect ratios and amplifies the stabilization. Similarly, inertia amplifies the stabilizing effect of neck-in as well, leading eventually to a window of unconditional stability within the domain of aspect ratios.

We could also explain the mechanisms underlying the stabilizing effect of inertia, gravity, and neck-in, including a simple argumentation based on steady state solutions and explaining the phenomenon of unconditional stability caused by inertia. The local Trouton ratios at inlet and outlet turned out to be the key for understanding the stabilizing influence of the aspect ratio. Finally, we checked the stability criteria of Kim and Jung for validity in presence of inertia, gravity, and neck-in. While Jung's criterion is limited to special cases, Kim's criterion is fulfilled in all situations. Based on the previous results for non-isothermal[12] and viscoelastic[28–30] settings, this is not surprising and suggests once more that the picture underlying this criterion covers the essence of the draw resonance mechanism.

It had been shown by Silagy, Demay, and Agassant[19] that the reduced model used in this work yields slightly different results than a general two-dimensional model. However, we used the simplified version in order to be able to perform a comprehensive linear stability analysis and to focus on the essential effects on the stability caused by finite film width. Experimental verifications of these results, at least up to the known inaccuracy of the model, would be of great interest for us, as, up to our knowledge, no study focusing on the influence of the aspect ratio exists. However, as most experiments are performed using viscoelastic fluids, the model has to be adapted accordingly in order to allow comparison, as viscoelasticity is well-known to have a large influence on the draw resonance behavior. This extension is left for future study.

ACKNOWLEDGMENTS

B.S. thanks the F.R.S.-FNRS and the IAP-7/38 MicroMAST project for supporting this research.

APPENDIX A: STEADY STATE VELOCITY OF THE VISCOUS-INERTIA MODEL IN THE PLANAR LIMIT

In the absence of gravity and for $a \to \infty$, Eqs. (13)-(15) can be reduced to the viscous-inertia model, i.e.,

$$\partial_t h + \partial_x(uh) = 0, \tag{A1}$$

$$Re\, h\,(\partial_t u + u\partial_x u) = 4\partial_x\,(h\partial_x u)\,, \tag{A2}$$

$Re = FQ$ being the Reynolds number.

Omitting the time derivatives, Eq. (A1) together with boundary conditions (8) directly yield $u_s = 1/h_s$ and Eq. (A2) can be written as

$$\partial_x\left(Re\, u_s - 4\frac{\partial_x u_s}{u_s}\right) = 0, \tag{A3}$$

which can be integrated to

$$Re\, u_s - 4\frac{\partial_x u_s}{u_s} = -c, \tag{A4}$$

c being an integration constant which has to be determined afterwards numerically so that $u_s(1) = Dr$ is fulfilled. Using partial fraction decomposition, this differential equation can be solved by basic integral calculus. Together with the inlet boundary condition $u_s(0) = 1$, we finally end up with

$$u_s(x) = \frac{c}{(c + Re)e^{-cx/4} - Re}. \tag{A5}$$

APPENDIX B: UNITY-THROUGHPUT WAVE TRAVELLING TIME

Based on the derivation given by Scheid *et al.*,[12] the calculation of the unity-throughput wave travelling time t_L is straightforward. The kinematic wave equation for a constant throughput $j = u\ell h$ is given by

$$\partial_t j + k\partial_x j = 0, \tag{B1}$$

where $k = k(x)$ denotes the phase speed of the wave. Using boundary conditions (8), the linearized throughput reads $j = 1 + Je^{\lambda t}$, with $J = U + L + H$, and the wave speed can be calculated with the help of (B1) and (17b) to

$$k = \frac{u_s J}{H + L}. \tag{B2}$$

As the wave corresponding to $j = 1$ is the only constant-throughput wave which travels the entire distance from the inlet to the outlet,[26] the corresponding unity-throughput wave travelling time can be calculated as

$$t_L = \int_0^1 \mathrm{d}x\ \mathrm{Re}\left(\frac{1}{k}\right) = \int_0^1 \frac{\mathrm{d}x}{u_s}\frac{((H_R + L_R)J_R + (H_I + L_I)J_I)}{(J_R^2 + J_I^2)}, \tag{B3}$$

where the subscripts "R" and "I" denote, respectively, the real and the imaginary parts.

[1] Y. L. Yeow, "On the stability of extending films: A model for the film casting process," J. Fluid Mech. **66**, 613–622 (1974).
[2] W. Minoshima and J. White, "Stability of continuous film extrusion processes," Polym. Eng. Rev. **2**, 211–226 (1983).
[3] N. R. Anturkar and A. Co, "Draw resonance in film casting of viscoelastic fluids: A linear stability analysis," J. Non-Newtonian Fluid Mech. **28**, 287–307 (1988).
[4] S. d'Halewyu, J. F. Agassant, and Y. Demay, "Numerical simulation of the cast film process," Polym. Eng. Sci. **30**, 335–340 (1990).
[5] V. R. Iyengar and A. Co, "Film casting of a modified Giesekus fluid: A steady-state analysis," J. Non-Newtonian Fluid Mech. **48**, 1–20 (1993).
[6] V. R. Iyengar and A. Co, "Film casting of a modified Giesekus fluid: Stability analysis," Chem. Eng. Sci. **51**, 1417–1430 (1996).
[7] M. Beaulne and E. Mitsoulis, "Numerical simulation of the film casting process," Int. Polym. Process. **14**, 261–275 (1999).
[8] S. Smith and D. Stolle, "Nonisothermal two-dimensional film casting of a viscous polymer," Polym. Eng. Sci. **40**, 1870–1877 (2000).

[9] G. Lamberti, G. Titomanlio, and V. Brucato, "Measurement and modelling of the film casting process 1. Width distribution along draw direction," Chem. Eng. Sci. **56**, 5749–5761 (2001).
[10] G. Lamberti, G. Titomanlio, and V. Brucato, "Measurement and modelling of the film casting process: 2. Temperature distribution along draw direction," Chem. Eng. Sci. **57**, 1993–1996 (2002).
[11] F. Cao, R. E. Khayat, and J. Puskas, "Effect of inertia and gravity on the draw resonance in high-speed film casting of Newtonian fluids," Int. J. Solids Struct. **42**, 5734–5757 (2005).
[12] B. Scheid, S. Quiligotti, B. Tran, R. Gy, and H. A. Stone, "On the (de)stabilization of draw resonance due to cooling," J. Fluid Mech. **636**, 155–176 (2009).
[13] B. Scheid, S. Quiligotti, B. Tran, and H. A. Stone, "Lateral shaping and stability of a stretching viscous sheet," Eur. Phys. J. B **68**, 487–494 (2009).
[14] M. Bechert, D. W. Schubert, and B. Scheid, "Practical mapping of the draw resonance instability in film casting of Newtonian fluids," Eur. J. Mech., B: Fluids **52**, 68–75 (2015).
[15] T. Dobroth and L. Erwin, "Causes of edge beads in cast films," Polym. Eng. Sci. **26**, 462–467 (1986).
[16] N. Satoh, H. Tomiyama, and T. Kajiwara, "Viscoelastic simulation of film casting process for a polymer melt," Polym. Eng. Sci. **41**, 1564–1579 (2001).
[17] K. Sakaki, R. Katsumoto, T. Kajiwara, and K. Funatsu, "Three-dimensional flow simulation of a film-casting process," Polym. Eng. Sci. **36**, 1821–1831 (1996).
[18] D. Silagy, Y. Demay, and J.-F. Agassant, "Study of the stability of the film casting process," Polym. Eng. Sci. **36**, 2614–2625 (1996).
[19] D. Silagy, Y. Demay, and J.-F. Agassant, "Stationary and stability analysis of the film casting process," J. Non-Newtonian Fluid Mech. **79**, 563–583 (1998).
[20] J. M. Kim, J. S. Lee, D. M. Shin, H. W. Jung, and J. C. Hyun, "Transient solutions of the dynamics of film casting process using a 2-D viscoelastic model," J. Non-Newtonian Fluid Mech. **132**, 53–60 (2005).
[21] D. Shin, J. Lee, J. Kim, H. Jung, and J. Hyun, "Transient and steady-state solutions of 2D viscoelastic nonisothermal simulation model of film casting process via finite element method," J. Rheol. **51**, 393–407 (2007).
[22] Z. U. Ahmed and R. E. Khayat, "Three dimensional film stability and draw resonance," J. Fluids Eng. **134**, 101302 (2012).
[23] R. E. Christensen, "Extrusion coating of polypropylene," SPE J. **18**, 751–755 (1962).
[24] J. C. Miller, "Swelling behavior in extrusion," Polym. Eng. Sci. **3**, 134–137 (1963).
[25] *Polymer Processing Instabilities: Understanding and Control*, edited by S. Hatzikiriakos and K. Migler (Marcel Dekker, New York, 2005).
[26] B. M. Kim, J. C. Hyun, J. S. Oh, and S. J. Lee, "Kinematic waves in the isothermal melt spinning of Newtonian fluids," AIChE J. **42**, 3164–3169 (1996).
[27] J. C. Hyun, "Theory of draw resonance: Part I. Newtonian fluids," AIChE J. **24**, 418–422 (1978).
[28] H. W. Jung and J. C. Hyun, "Stability of isothermal spinning of viscoelastic fluids," Korean J. Chem. Eng. **16**, 325–330 (1999).
[29] H. W. Jung, H.-S. Song, and J. C. Hyun, "Draw resonance and kinematic waves in viscoelastic isothermal spinning," AIChE J. **46**, 2106–2111 (2000).
[30] J. S. Lee, H. W. Jung, J. C. Hyun, and L. E. Scriven, "Simple indicator of draw resonance instability in melt spinning processes," AIChE J. **51**, 2869–2874 (2005).
[31] H. W. Jung, S. M. Choi, and J. C. Hyun, "Approximate method for determining the stability of the film-casting process," AIChE J. **45**, 1157–1160 (1999).
[32] E. Doedel, A. Champneys, T. Fairgrieve, Y. Kuznetsov, B. Sandstede, and X. Wang, "AUTO97 continuation and bifurcation software for ordinary differential equations," 1997, AUTO software is freely distributed on http://indy.cs.concordia.ca/auto/.
[33] W. W. Schultz and S. H. Davis, "Effects of boundary conditions on the stability of slender viscous fibers," J. Appl. Mech. **51**, 1–5 (1984).
[34] M. Renardy, "Draw resonance revisited," SIAM J. Appl. Math. **66**, 1261–1269 (2006).
[35] Some authors use a reciprocal definition of the aspect ratio.[18,20,21]
[36] Note that the fluidity F is defined here in a slightly different manner than in our previous work,[14] as the Trouton ratio, which is always 4 in the latter case, is not constant here and therefore cannot be included in the definition.
[37] The stability map presented in our previous work[14] differs slightly from the one shown here, as the definition of the fluidity differs by a factor of 4.
[38] Note that a complete suppression of draw resonance does not always imply that steady processing is technically achievable, as the strong acceleration near the outlet in the case of high inertia force leads to strong tension within the fluid, which may lead to film break-up.
[39] Strictly speaking, the term "unity-throughput" is only correct for $Q = 1$ and "Q-throughput" would be more adequate in general, as according to boundary conditions (7), the steady throughput is equal to Q. Nevertheless, we keep the term consistent with Kim *et al.*,[26] as we will use exclusively the alternative scaling with boundary conditions (8) throughout this section.